

See discussions, stats, and author profiles for this publication at: <https://www.researchgate.net/publication/334441320>

# Using Landsat observations (1988–2017) and Google Earth Engine to Detect Vegetation Cover Changes in Rangelands – A First Step Towards Identifying Degraded Lands for Conservation

Article in *Remote Sensing of Environment* · July 2019

DOI: 10.1016/j.rse.2019.111317

---

CITATIONS

29

7 authors, including:



Zunyi Xie

The University of Queensland

20 PUBLICATIONS 227 CITATIONS

[SEE PROFILE](#)

READS

2,100



Stuart Phinn

The University of Queensland

525 PUBLICATIONS 13,723 CITATIONS

[SEE PROFILE](#)



Edward T Game

The Nature Conservancy

112 PUBLICATIONS 4,402 CITATIONS

[SEE PROFILE](#)



David J. Pannell

University of Western Australia

319 PUBLICATIONS 9,759 CITATIONS

[SEE PROFILE](#)

Some of the authors of this publication are also working on these related projects:



Australia Sea Level Rise Project [View project](#)



Pantanal Coexistence Lab [View project](#)



# Using Landsat observations (1988–2017) and Google Earth Engine to detect vegetation cover changes in rangelands - A first step towards identifying degraded lands for conservation



Zunyi Xie<sup>a,b,c,\*</sup>, Stuart R. Phinn<sup>c</sup>, Edward T. Game<sup>d</sup>, David J. Pannell<sup>e</sup>, Richard J. Hobbs<sup>f</sup>, Peter R. Briggs<sup>g</sup>, Eve McDonald-Madden<sup>b</sup>

<sup>a</sup> Key Laboratory of Geospatial Technology for the Middle and Lower Yellow River Regions, Ministry of Education, Henan University, Kaifeng 475004, China

<sup>b</sup> Centre for Biodiversity and Conservation Science, School of Earth and Environmental Sciences, The University of Queensland, Brisbane, Queensland 4072, Australia

<sup>c</sup> Remote Sensing Research Centre, School of Earth and Environmental Sciences, The University of Queensland, Brisbane, Queensland 4072, Australia

<sup>d</sup> The Nature Conservancy, South Brisbane, QLD 4101, Australia

<sup>e</sup> School of Agriculture and Environment, The University of Western Australia, Crawley, WA 6009, Australia

<sup>f</sup> School of Biological Sciences, The University of Western Australia, Crawley, WA 6009, Australia

<sup>g</sup> CSIRO Oceans and Atmosphere, Canberra, ACT 2601, Australia

## ARTICLE INFO

Edited by Jing M. Chen

Keywords:

Vegetation cover

Rangelands

SDGs

Big data

Landsat

Google Earth Engine

## ABSTRACT

Globally, the area of agricultural land is shrinking in part due to environmental degradation. Acquisition and restoration of degraded lands no longer used for agriculture may present a major conservation opportunity with minimal social and political opposition. The ability to efficiently and accurately identify these lands from regional to global scales will aid conservation management, ultimately enhancing the global prospects of achieving the Sustainable Development Goals (SDGs). Remote Sensing provides a potential tool to identify areas where surface property changes can be mapped and linked with land degradation. In this study, we begin to tackle a small section of this challenge by presenting novel approach to mapping changes in vegetation cover amounts at the pixel level (30 m), using Google Earth Engine (GEE). We illustrate our approach across large-scale rangelands in Queensland Australia, using three decades of Landsat satellite imagery (1988–2017) along with field observations of land condition scores for validation. The approach used an existing method for dynamic reference cover to remove the rainfall variability and focused on the human management effects on the vegetation cover changes.

Results showed the identified vegetation cover changes could be categorized into five classes of decrease, increase or stable cover compared with a set reference level, which was obtained from locations of the most persistent ground cover across all dry years. In total, vegetation cover decrease was observed in 20% of our study area, with similar portion of lands recovering and the rest (~60%) staying stable. The lands with decrease in vegetation cover, covering a considerable area of  $\sim 2 \times 10^5 \text{ km}^2$ , exhibited a markedly reduced resilience to droughts. The accuracy assessment yielded an overall classification accuracy of 82.6% ( $\pm 3.32$  standard error) with 75.0% ( $\pm 5.16\%$ ) and 70.0% ( $\pm 4.13\%$ ) producer's and user's accuracy for areas experiencing a significant decrease in vegetation cover, respectively. Identifying areas of degraded land will require multiple stages of spatial data analysis and this work provided the first stage for identifying vegetation cover changes in large-scale rangeland environment, and provides a platform for future research and development to identify degraded lands and their utility for achieving conservation endeavours.

## 1. Introduction

Biodiversity is being lost at an alarming rate (Butchart et al., 2015), making conservation a significant national and global issue, with many high profile papers cataloguing the contribution of protected areas

(Watson et al., 2014), what additional conservation is required to meet international targets (Venter et al., 2014), and where priorities for doing so should be (McDonald-Madden et al., 2011). Much contemporary conservation happens in highly contested space; places that are important for biodiversity but also economically valuable for

\* Corresponding author at: Centre for Biodiversity and Conservation Science (CBCS), The University of Queensland, Brisbane, QLD 4072, Australia.

E-mail address: [z.xie@uq.edu.au](mailto:z.xie@uq.edu.au) (Z. Xie).

agriculture, mining, or housing and infrastructure development. Conservation outcomes in these places are often limited by the difficulty of navigating numerous competing interests and values. On the other hand, the changing nature of land condition over time, such as loss of productive vegetation cover, can potentially lead to lower land values, and minimal social and political opposition to conservation activities. As one example, a dramatic decline in agricultural productivity due to land degradation has resulted in 12 million hectares of global arable land being left abandoned annually (IPBES, 2018). While restoration of low productivity, low condition or degraded lands could be expensive, the lack of competition for their use may mean that they offer an efficient way of adding to the global conservation estate (Poore, 2016; Possingham et al., 2015). To capitalise on the conservation potential of these lands at large scales (regional or global) we must first identify their extent and location. This paper presents a first step to address this challenge, by establishing a method that could work across one of our largest global terrestrial land-use types.

Satellite image data provide a potential tool to aid in identifying areas where changes in surface properties can be mapped and linked with multiple signs of land condition change. From this point carefully defined thresholds can be used to define levels of land degradation, a step requiring specific field knowledge and often application dependent. Research efforts to reliably map and monitor changing land condition and degradation via land surface and vegetation changes remain a major and open challenge (Vogt et al., 2011). Previous studies to mapping land degradation, assess actual and potential changes in soil and vegetation cover amounts, then apply multiple criteria to set thresholds for types and degrees of degradation (Dregne, 2002; Gibbs and Salmon, 2015). These approaches have included expert opinion (Batjes, 2001; Oldeman et al., 1990; Sommer et al., 2011), empirical observation (Ajmi et al., 2014; Andeltova et al., 2013; Muir et al., 2011), and biophysical modelling (Cai et al., 2010; Hubacek and Sun, 2001; Turner et al., 2016).

Remote Sensing and spatial modelling have been increasingly used since 2000 to develop measures of surface properties, which are then analysed to assess degradation (Tewkesbury et al., 2015; Bai et al., 2008; Holm, 2003; Vicente-Serrano et al., 2015a). Even though there have been some applications in measuring soil conditions using Remote Sensing (Caccetta et al., 2010; Furby et al., 2010; Lobell, 2010), it remains challenging for satellites to directly sense soil dynamics. While vegetation cover is the current most widely used indicator, it sometimes can be confounded by invasive vegetation (Hestir et al., 2008). The majority of these previous approaches have used coarse spatial resolution pixels (e.g. NOAA-AVHRR), which often lacked sufficient details to allow comparison against empirical observations, leading to difficulty in evaluating mapping methods (Helldén and Tottrup, 2008; Wessels et al., 2007). As yet efforts to assess land degradation at finer spatial resolutions ( $< 250$  m), they have been restricted to small areas ( $< 3 \times 10^4 \text{ km}^2$ ) due to data storage and computing challenges (Bastin et al., 2012; Eckert et al., 2015; Hansen and Loveland, 2012; Johansen et al., 2015; Kennedy et al., 2014; Mariano et al., 2018). Even when such fine spatial scale maps are produced, understanding changes in surface properties, and any ability to assess degradation from these areas, is further complicated by an inability to distinguish human impacts from changes in surface properties due to inter-annual rainfall variability and trends (Hein et al., 2011; Wessels et al., 2012). Without moving towards approaches and tools that can delineate surface property changes at large spatial scales, with high resolution, using up-to-date information, and segregation of rainfall affects, our ability to assess condition and define degradation in a way to inform conservation planning decisions is limited. Google Earth Engine (GEE), an online cloud-computing platform that holds a multi-petabyte catalog of satellite imagery and geospatial datasets (Gorelick et al., 2017), can facilitate planetary-scale analysis of Remote Sensing big data and offers an unprecedented opportunity to advance our scientific understanding of various dynamic processes associated with earth systems,

particularly land change science (e.g. Donchyts et al., 2016; Hansen et al., 2013; Pekel et al., 2016).

In this study, we piloted a novel set of methods, including dynamic reference cover methods and drought index, for mapping changes in surface vegetation properties with GEE, while removing the confounding effects of rainfall dynamics. We tested our approach in a large rangeland area ( $\sim 1.0 \times 10^6 \text{ km}^2$ ,  $\sim 1.7$  billion pixels) in Queensland Australia, an environment on which many species and societies rely and home in (Ludwig and Tongway, 2002) with known validation and application datasets. Using three decades (1988–2017) of Landsat satellite observations combined into 3-month seasonal composites (Gill et al., 2017), we were able to identify the change in vegetation cover at a 30 m resolution across our study area.

## 2. Data and methods

### 2.1. Study area

Occupying  $\sim 50\%$  of the global land area, rangelands provide important ecosystem services such as provisioning (forage for livestock and wild animals, land for farming), support (soil formation and conservation, nutrient cycling), water and climate regulation, and culture (e.g., cultural identity and diversity, aesthetics, tourism). Rangelands generally consist of grass, shrub, and savannah vegetation types within dry subhumid to hyper-arid areas (Bastin et al., 2012). A relatively large proportion of world's areas with poverty (e.g. low energy supply, food insecurity) and conservation threats are located in rangelands (Bedunah and Angerer, 2012). Therefore, understanding the changes and dynamics of rangeland resources is becoming increasingly important for the global Sustainable Development Goals (SDGs). However, the large extent of rangelands, combined with their spatial complexity and temporal variability pose challenges for routinely monitoring their vegetation cover conditions (Karfs et al., 2009a; Watson et al., 2007).

In this study, we chose rangelands in Queensland (QLD) Australia as a pilot study area (Fig. 1A), which include grazing trails for building the vegetation cover mapping approach and extensive field data for validation. Rangelands take up over 80% of Queensland ( $\sim 1.4 \times 10^6 \text{ km}^2$ ) and extend across the arid southwest inland to the seasonally high rainfall areas in the north-east (orange area in the inset of Fig. 1A). These lands are characterised by an extreme transition in precipitation with mean annual rainfall increasing dramatically from  $< 200$  mm in the arid interior to over 2 m on the far north of the state (Fig. 1B). Land cover types over Queensland rangelands form a diverse group of relatively undisturbed ecosystems such as tropical savannas, woodlands, shrublands and grasslands (Fig. 1C) across nine bioregions with a diversity of habitats and ecological communities (Fig. 1A). Our proposed approach for assessing land surface change will be based on the Dynamic Reference Cover Method (DRCM) developed by Bastin et al. (2012) and focus on vegetation cover change in relation to specific reference conditions. As a result, it will not work in specific sections of Queensland's rangelands, which have changes in cover due to specific environmental dynamics (channel country, mangroves, wet tropics) or human activities (broad-acre cropping and vegetation clearing). We excluded all these areas to make sure our method is accurately used. At last, the study area where our methods were applied, covers around 75% of the Queensland rangelands ( $1.0 \times 10^6 \text{ km}^2$ , colourful areas in Fig. 1A).

A key part of our study area for use in validation is the Wambiana grazing trial. It was established in December 1997, is located on low-fertility tertiary sediments (typical northern Australia land type) on the Wambiana pastoral lease ( $20.54^\circ \text{ S}$ ,  $146.13^\circ \text{ E}$ ) in the northeast of Queensland (Fig. 1A, D). It is an ongoing project with objectives to compare the performance of different grazing strategies in a savanna woodland to generate empirical evidence for better commercial grazing-management (O'Reagain et al., 2009). Prior to its establishment, the trial area was grazed as part of a larger surrounding

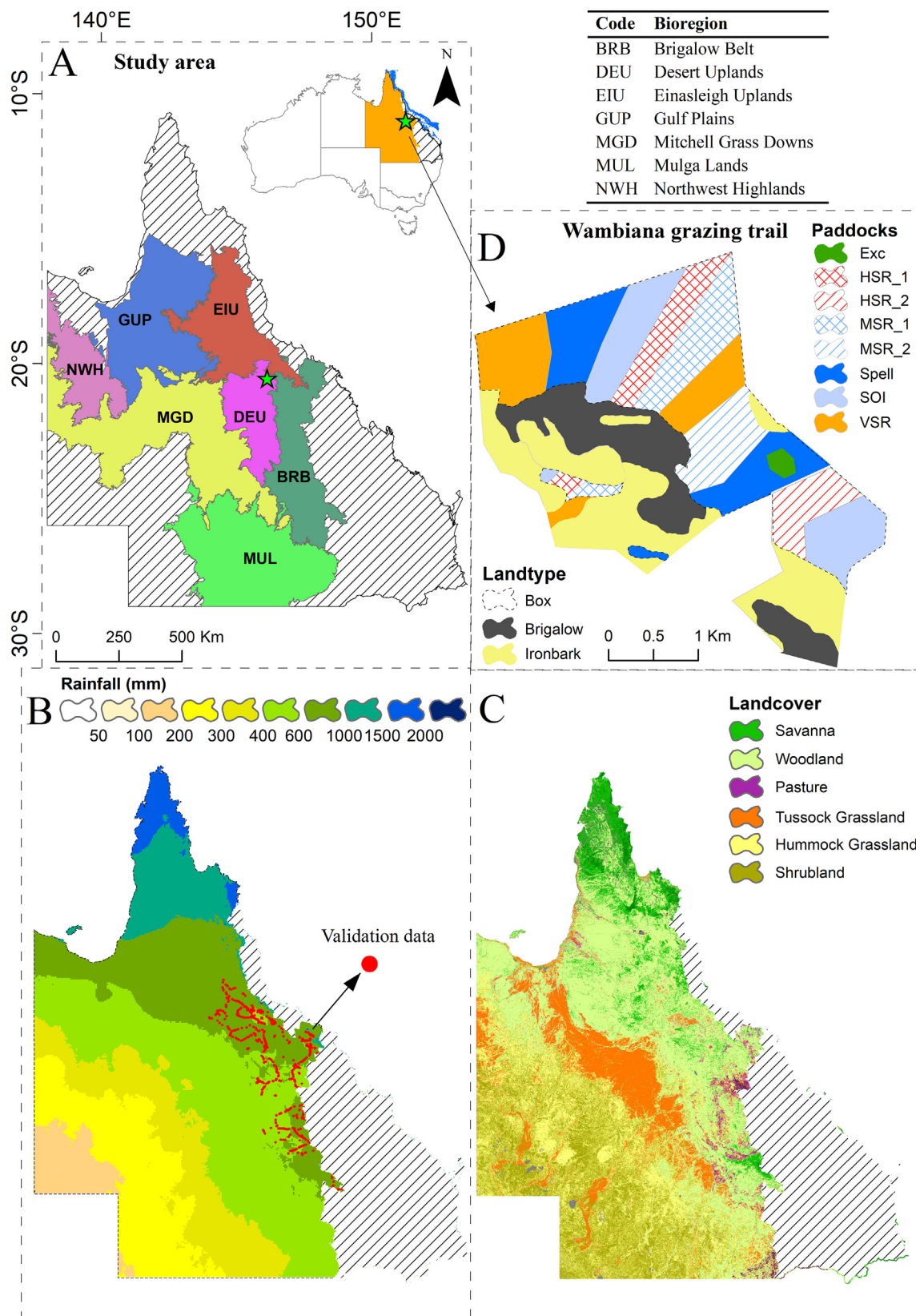


**Fig. 1.** (A) Study area in Queensland highlighted by bioregions (table) with colours and the orange area in the inset indicates the rangelands. (B) Rainfall over rangelands (BoM) with validation data. (C) Land cover over rangelands (DLCD) and (D) Wambiana grazing trial (O'Reagain and Bushell, 2015). (For interpretation of the references to colour in this figure legend, the reader is referred to the web version of this article.)

**Table 1**

Classification of A, B, C, and D land conditions with soil, pasture, weed and woodland components (Karfs et al., 2009b).

Landscape quality features		
Landscape component	Positive qualities	Negative qualities
Soil	High levels of organic material and good soil structure	Erosion
Pasture	Density and coverage of preferred grasses (perennial, productive, palatable)	Few preferred species
Weeds	No sign of weeds	Increasing weed density
Woodland	No sign or only early signs of woodland thickening	Increasing woody density

Condition rating			
A	<ul style="list-style-type: none"> <li>• High density and coverage of preferred grasses</li> <li>• High organic matter</li> </ul>	B	<ul style="list-style-type: none"> <li>• Moderate density and coverage of preferred grasses or high density of intermediate grasses</li> <li>• Moderate organic matter</li> </ul>
C	<ul style="list-style-type: none"> <li>• Moderate to low density of preferred grasses or moderate density of intermediate grasses</li> <li>• Higher numbers of annual grasses and forbs, few weeds</li> <li>• Some erosion</li> <li>• Some woody thickening</li> </ul>	D	<ul style="list-style-type: none"> <li>• General lack of any perennial grasses or forbs</li> <li>• Severe erosion and large bare areas</li> <li>• High numbers of weeds/annuals</li> <li>• Thickets of woody plants covering much of the area</li> </ul>

commercial paddock. Five grazing treatments, assessing the effects of different cattle stocking rates in response to climate, have been replicated across three soil types within each of the 100 ha paddocks along with a small area of enclosure (Fig. 1D). This region experiences a mean annual precipitation of ~690 mm and mean annual temperature of ~23°. The three areas we used to assess changes in vegetation cover were the enclosure (Exc) area, and paddocks with heavy (HSR) and moderate (MSR) stocking rates.

## 2.2. Landsat time series and seasonal composite data

Thirty years (1988–2017) of Landsat surface reflectance data (Tier 1, Collection 1) were used in this study, which have been corrected for atmospheric, reflectance, topographic and satellite sensor effects (Flood, 2013). Spatially, 64 Landsat scenes from World Reference System path 92–101 and row 70–80 were required to mosaic and cover the entire study area. In total over 20,000 images of different sensors were initially obtained from Google Earth Engine's data catalog, including the Landsat Thematic Mapper (TM, Landsat 4–5), the Enhanced Thematic Mapper Plus (ETM+, Landsat 7) and the Operational Land Imager (OLI, Landsat 8) with 16 days and 30 m resolutions. Undesirable elements such as cloud, cloud shadow, aerosol and inundation were further masked from all the images based on the quality assessment flags provided in the Tier 1 product (Goodwin et al., 2013; Zhu and Woodcock, 2012). These image processes ensure comparisons over space and time are consistent and repeatable, and any changes detected are representative of true change instead of artefacts or spurious measurements in the imagery. Lastly, all data were temporally aggregated into 118 Australian seasonal composites of Summer (December–February), Autumn (March–May), Winter (June–August) and Spring (September–November). This was done by determining the medoid of three months (a season) of the imagery, which is a multi-dimensional equivalent of the median that minimises the total distance between the selected point and all other points. In this way, the acquired medoid is a specific data point instead of an averaged or blended value, which is robust against extreme values, inherently avoiding the selection of outliers (Flood, 2013). These seasonal data can minimize the missing data and cloud contamination present in single date imagery and to create a regular temporal sequence, which is well suited to time-series analysis applications like this study (Scarth et al., 2015).

## 2.3. Hydro-meteorological data

To take into account seasonal and long-term rainfall patterns (1988–2017) across our study area, we used the Australian Bureau of

Meteorology's (BoM) 'recalibrated' daily rainfall product (Jones et al., 2009; Australian Bureau of Meteorology, 2018). This is a gridded interpolation to 0.05° resolution (~5 km) of the records from a national network of precipitation gauges, which can include between 1272 and 2043 operating in QLD during the period.

Priestley-Taylor (Priestley and Taylor, 1972) potential evapotranspiration estimates (PET) from 1988 to 2017 were outputs (at the same resolution) of the Australian Water Availability Project's (AWAP) WaterDyn model (Raupach et al., 2009; Raupach et al., 2018). The WaterDyn model formulation uses daily BoM downward solar and air temperature, and Swinbank (1963) downward longwave radiation. Daily BoM rainfall and AWAP PET were further aggregated into monthly data and combined to calculate a physically-based drought index as a measure of historical dry conditions over the study area.

## 2.4. Validation data

The biophysical field observations of land conditions (Karfs et al., 2009b), representing specific type of vegetation cover and soil change, were used for accuracy assessment (Department of Environment and Science, Queensland government). In total over 1500 records were collected along roads through rangelands as a 1 km buffer during the periods from 2004 to 2012 within the Burdekin Dry Tropics region in northeast Queensland, which covers an area of approximately 8% of the state and over half is located in our study area. This land condition framework provides differentiation between land condition classes that were categorized based on grazing land ecology and research from long-term grazing trials in the Burdekin Dry Tropics (Karfs et al., 2009b). Land condition in the framework is defined as 'the ability of land to respond to rain and produce useful forage', with four classes: A and B represent stable land condition or vegetation cover, C stands for a potential decline in land condition or vegetation cover that is susceptible to falling to D condition and may require a significant change in the land management, and D indicates significant decline in land condition, the reversal of which will require major management action. Land condition discussed here is a multifaceted assessment, to arrive at the classification of A, B, C or D condition, combinations of key positive and negative features of the region's soil, pasture, weed and woodland components were considered (Table 1). This had involved in assessment criteria of pasture density and types, vegetation ground cover, soil condition (crust broken-ness, erosion features and deposited materials), introduced weeds, trees as well as additional information on grazing, yield, assessors and comments. More details can be found in the guide of land condition assessment for Burdekin region with photo standards (Karfs et al., 2009b).

## 2.5. Land cover and use maps

Dynamic Land Cover Dataset (DLCD) was used as the source of the land cover classifications over the study area (Lymburner et al., 2011). This land cover map (Fig. 1C) was developed from an analysis of a 16-day EVI composite collected at 250 m resolution using the Moderate Resolution Imaging Spectroradiometer (MODIS) satellite for the period from 2000 to 2008 (Huete et al., 2002; Zhang and Foody, 1998). The DLCD classification scheme conforms to the International Standards Organisation (ISO) land cover standard, with classes from cultivated and managed land covers (crops and pastures) to natural land covers such as closed forest and sparse, open grasslands (Lymburner et al., 2011). The most recent land use map from the Australian Land Use and Management Classification (ALUMC) in 2016 was used to exclude undesired regions from the study area such as water, urban, and croplands and so on (ABARES, 2015). Five primary classes were identified and structured at 50 m resolution by the potential degree of human modification and impact on a ‘nature state’ (essentially, a native land cover).

## 2.6. Dynamic reference cover method

In order to distinguish human-induced vegetation cover changes from those due to inter-annual variability in rainfall, the Dynamic Reference Cover Method (DRCM) developed by Bastin et al. (2012) was used (Fig. 2). Vegetation ground cover data, here we refer to Ground Cover (GC), were extracted from ‘green’ and ‘non-green’ components of the Landsat-derived seasonal fractional ground cover and used as the basics for DRCM. GC data represent both the photosynthetic vegetation and non-photosynthetic brown or senescent vegetation, such as litter, dead leaf and branches in percent (no unit). Based on the GC multi-temporal image sequence, DRCM was applied via a neighborhood search window with a suggested size of 1500 × 1500 Landsat pixels (Fig. 2A). It first excluded the pixels with woody cover > 60% and extracted the β-distribution fitted minimum ground cover image, which represents the most persistent ground cover in years of lowest rainfall (Fig. 2B). The 90–95 percentile of the minimum ground cover image was then used to identify the reference-pixel locations for the focal pixel, which can largely reduce the persistent cover in higher percentile (> 95%) on run-on features, creek beds, hillslopes and so on (Fig. 2C). Lastly, we calculated the rainfall adjusted ground cover ( $\Delta GC$ ) for the focal pixel of each search window (Fig. 2D) as:

$$\Delta GC(t) = GC(t)_{focal} - GC(t)_{ref} \quad (1)$$

where t represents each season of the time series and  $\Delta GC(t)$  is computed as the difference in ground cover between the central focal pixel  $\Delta GC(t)_{focal}$  and the averaged surrounding reference pixels  $\Delta GC(t)_{ref}$  in the search window.

This provides an estimate of how well the focal pixel is performing compared with surrounding areas that represent a ‘best available’ reference condition. We computed  $\Delta GC$  of each pixel for all of the seasonal images by stepping through the search window on the GC multi-temporal image stack. By assessing the trend in the time series of  $\Delta GC$  images for each pixel area (30 m) over the successive drought years, the vegetation ground cover changes can be assessed due predominantly to anthropogenic land management (Bastin et al., 2012).

We modified and updated the method in order to create the seasonal DRCM data which best fit for QLD rangeland environment with high processing efficiency (Scarth et al., 2015; Scarth et al., 2010). The major bottleneck, stepping through a 1500 × 1500 pixels (30 m) window on a per pixel basis to determine the reference cover points is very intensive. This routine was rewritten in optimized Fortran code and was wrapped as a python function. This resulted in a speedup of 1000 times. Furthermore, the Ground Cover Index image used in the previous method (Bastin et al., 2012) was calculated from seasonal fractional cover product, which does not distinguish tree, mid-level woody foliage and branch cover from green and dry ground cover,

confining the DRCM method to only areas with woody vegetation < 15% (Scarth et al., 2006). We improved this by using seasonal fractional Ground Cover (GC) data derived from a model that used the total vegetation cover and the estimated ‘persistent’ cover (i.e. that from woody canopies) to estimate the fractional ground cover under woody canopies (Gill et al., 2017). The separation of the ‘persistent green’ from the total cover product, allows for the adjustment of the underlying spectral signature of the fractional cover image and the creation of a resulting ‘true’ ground cover estimate for each season. This led to a ‘true’ ground cover and enables pixels to be used in areas with up to 60% woody foliage cover (Flood, 2013; Trevithick et al., 2014). In addition, reference pixels on certain landforms (hills, jump ups, undulating plains etc.) across our study area were excluded from the analysis via terrain classification, as well as the pixels where the land clearing occurred based on the Statewide Landcover and Trees Study observations (Muir et al., 2011; Trevithick et al., 2012). The final DRCM imagery produced in this study consists of two variables at each pixel location, including 1) the rainfall adjusted ground cover, i.e. vegetation ground cover change ( $\Delta GC$  = pixel GC value – mean GC value of reference pixels + 100), which separates human ground cover management effects and rainfall variability; and 2) the reference ground cover, which represents the pixels with the most persistent vegetation ground cover across all dry years. Although DRCM was used with confidence over most of our study area, there may still be uncertainties in it for identifying reference/benchmark sites over some areas due to 1) the position in the landscape and 2) different land types for the reference and target sites. Despite the 90–95 percentile of the minimum ground cover image and a moving window of 1500 × 1500 pixels being used to minimize the uncertainties, future work is still needed to tackle these limitations.

## 2.7. Drought index calculation

Due to its size, there is significant diversity of climate patterns with highly variable rainfall across rangelands in QLD. Thus, it is unrealistic to select fixed dry and wet periods for ground cover trend analysis for the entire study area. To better characterize the climate condition at regional scale across time and space, a drought index is required to identify successive dry periods at a pixel level. We chose to use the Standardized Precipitation-Evapotranspiration Index (SPEI), which is a multi-scalar drought metric (i.e., monthly, seasonally, half-yearly, and annual) based on climatic data (Vicente-Serrano et al., 2010). It can be used for determining the onset, duration and magnitude of different drought types with respect to normal conditions in a variety of natural and managed systems in the context of global warming (Beguería et al., 2014; Vicente-Serrano et al., 2015b).

The existing global SPEI dataset available for public use has a coarse spatial resolution of 0.5°, and only covers the period from 1901 up to 2015. In this study, we used monthly BoM rainfall and AWAP PET to recalculate the SPEI-3 (seasonal integration) from 1988 to 2017 with a much higher resolution of 5 km, which is better suited to Australian climate conditions. The main steps for calculating seasonal SPEI were as follows (Han et al., 2018):

- 1) The seasonally accumulated difference between precipitation and PET was calculated as:

$$D_i = P_i - PET_i \quad (2)$$

$$D_3 = \sum_{i=0}^{k-1} \left[ \frac{2(i+1)}{k(k+1)} (P_{n-i} - PET_{n-i}) \right], n \geq k \quad (3)$$

where  $D_i$  is water surplus or deficit for the analysed  $i^{\text{th}}$  month (mm);  $P_i$  and  $PET_i$  are the  $i^{\text{th}}$  month precipitation and PET (mm);  $D_3$  represents the accumulated  $D_i$  at seasonal time scale based on linearly decreasing weight;  $k$  is the time scale ( $k = 3$  months) and  $n$  is the number of total monthly data used;

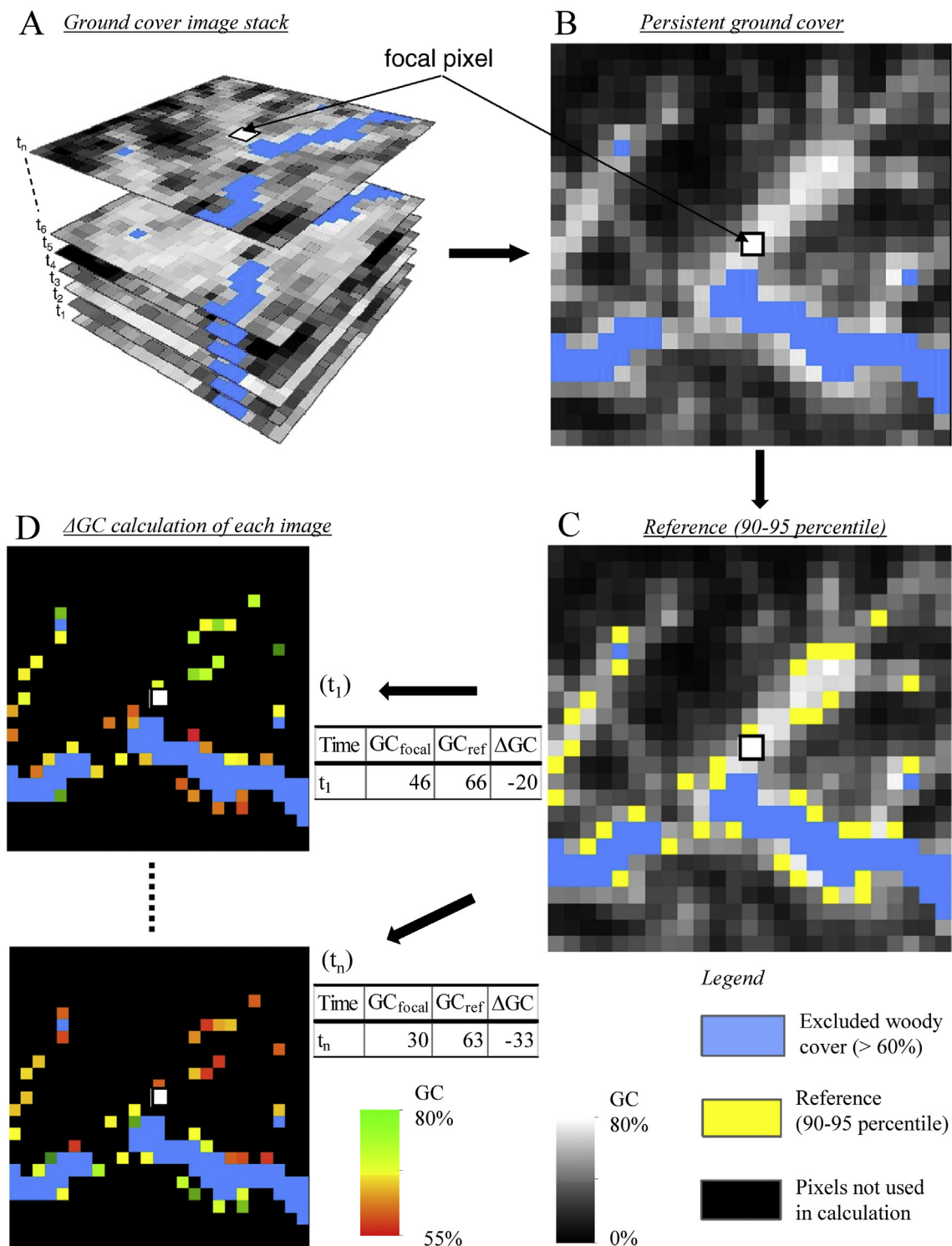


**Fig. 2.** Example of dynamic reference cover method to calculate rainfall adjusted vegetation ground cover ( $\Delta GC$ ) for the focal pixel of a neighborhood search window, which was recommended as size of  $1500 \times 1500$  pixels (30 m) but illustrated here as an enlarged 100 pixel and line subset (modified from Bastin et al., 2012). (A) The multi-temporal image sequence of ground cover. (B) Persistent ground cover with blue pixels indicating excluded areas where woody cover > 60%. (C) Reference-pixel locations (yellow colour) derived from 90 to 95 percentile of persistent ground cover. (D) Calculation of  $\Delta GC$  for the focal pixel in each neighborhood search window and across all the seasonal images. (For interpretation of the references to colour in this figure legend, the reader is referred to the web version of this article.)

2) The probability distribution function of  $D_3$  according to the Log-logistic distribution is then given as:

$$F(D_3) = \left[ 1 + \left( \frac{\alpha}{1 - \gamma} \right)^\beta \right]^{-1} \quad (4)$$

where  $\alpha$ ,  $\beta$ , and  $\gamma$  are the scale, shape, and origin parameters, which were derived by the L-moment method (Ahmad et al., 1988; Singh

**Table 2**  
Categorization of drought/humid graded by the SPEI values.

Categories	SPEI values
Extreme drought	< -2.0
Severe drought	(-2.0, -1.5]
Moderate drought	(-1.5, -1.0]
Mild drought	(-1.0, -0.5]
Near normal	(-0.5, 0.5]
Humid/wet	> 0.5

et al., 1993).

3) SPEI was eventually calculated as the standardized values of  $F(x)$ :

$$SPEI = w - \frac{c_0 + c_1w + c_2w^2}{1 + d_1w + d_2w^2 + d_3w^3}, P \leq 0.5, P = 1 - F(x) \quad (5)$$

$$SPEI = -\frac{c_0 + c_1w + c_2w^2}{1 + d_1w + d_2w^2 + d_3w^3}, P > 0.5, P = 1 - P \quad (6)$$

where  $w = -2\ln(P)$  and the constants are:  $c_0 = 2.515517$ ,  $c_1 = 0.802853$ ,  $c_2 = 0.010328$ ,  $d_1 = 1.432788$ ,  $d_2 = 0.189269$ ,  $d_3 = 0.001308$ .

With the produced SPEI, the drought severity was classified over each 5 km pixel location across the study area. The drought classification adopted in this study is defined in Table 2 with more negative values indicating more severe drought (Aadhar and Mishra, 2017; Han et al., 2018).

## 2.8. Vegetation cover change mapping

Before assessing vegetation ground cover changes across the whole study area, we first tested the methods discussed below and developed the mapping approach over the 'Wambiana grazing trial' in far north Queensland, that has paddocks under known land conditions (Fig. 1D). Here we identified five possible types of vegetation cover change. We focused on identifying the changes in total vegetation on the ground and the conceptual diagram of the vegetation cover change mapping in this study is depicted in Fig. 3, of which the output map can be used to set user-specified threshold for land condition or degradation.

The key methods are as follows: First, rainfall adjusted ground cover ( $\Delta GC$ ) time series at pixel level across Wambiana was filtered into two different time periods, representing ① time series of winter during both dry and wet years (DRCM data was produced based on the ecological principle of stability of perennial herbage from benchmark areas, the  $\Delta GC$  is best presented in the winter season in QLD); ② time series of all successive dry periods where SPEI is less than -0.5, indicating a drought status with respect to the normal condition (Table 2). Next, the trend analysis was achieved via a sliding-window method, which applied a rolling window of 15 years (½ length of the time series, 59 seasonal values) to the two selected time series. A simple linear regression was calculated for each pixel on rolling-window  $\Delta GC$  values by sliding one time step each time. The acquired piecewise trends over all time steps for each pixel were then averaged to produce the two final trend maps (Fig. 3E). The change in  $\Delta GC$  is represented by the mean slopes and significance ( $P$ -value < 0.05). This technique was chosen to reduce the influence of outliers and highlight longer-term trends. Lastly, the following decision rules were uniformly applied to all pixels of the two trend maps to define the five vegetation cover change classes (Fig. 3E): pixels with significant decreasing trends in both time periods of ① and ② as 'Significant decrease' class, those that had significant downward trend in all dry periods (②) but switched into non-significant trend in both dry and wet periods (①) were defined as 'Potential decrease' class. Likewise, pixels allocated into 'Significant increase' class were those had significant increasing trends in both time periods of ①

and ② while pixels with significant upward trend only in period ① but stayed stable during all dry periods (②) were classified as 'Potential increase' class. The remaining pixels have stable vegetation ground cover profiles similar to those of reference pixels were assigned as 'Stable' class.

Previous studies have shown that the human effect of management strategies in actual ground cover space could be dwarfed by environmental climate (Scarth et al., 2010). Even though rainfall variability has been removed in this study by the DRCM method, a reduction of 20% in ground cover is still required before a significant negative linear slope was apparent (Wessels et al., 2012). To solve this issue, we conducted correlation analysis between DRCM- $\Delta GC$  data and rainfall, of which a significant correlation indicates human intervention. This can potentially pick up pixels with non-significant decreasing trends due to  $\Delta GC$  reduction of < 20% but were actually affected by human management, and we further reclassified them from 'Stable' class to 'Potential decrease' class. In addition, a method for calculating accumulation of DRCM- $\Delta GC$  was undertaken to filter out pixels with a non-significant positive trend but had significant accumulative positive increase in  $\Delta GC$  throughout the study time. These pixels were then reclassified from 'Stable' class to 'Potential increase' class.

After testing, modifying and updating the mapping methods over the 'Wambiana grazing trial', the final vegetation cover change mapping approach was eventually established. It was further extended and applied to the whole study area to produce the final vegetation cover change map with five classes from non-decrease ('Stable', 'Potential increase' and 'Significant increase') to decrease ('Potential decrease' and 'Significant decrease') classes. Irrelevant areas such as residential, industrial and farm infrastructure and so on were excluded from the analyses using land use map.

## 2.9. Accuracy assessment

The mapping accuracy in this study was systematically and quantitatively evaluated by using population error matrix also known as area adjusted confusion matrix (Foody, 2002; Congalton, 1991). Different from the sample error matrix, the population error matrix is constructed when both the reference and image classifications for all areas on the map are available (Liu et al., 2007) and where  $P_{ij}$  in the error matrix (Table 3) represents the proportion of area in the mapped class i and the reference class j. Population error matrix can improve the classification accuracy assessment by reducing the occurrence of the rare class in the sample through the class area correction. The classification accuracies of our vegetation cover change map including overall accuracy, user's accuracy and producer's accuracy, along with the standard errors of the estimators were estimated by the matrix and the equations (Table 3) below (Ayala-Izurieta et al., 2017; Olofsson et al., 2014):

This accuracy assessment was achieved by validating the classified map against the independent sample of land condition scores over our study area region, covering an area of 69,000 km<sup>2</sup>. The biophysical field observations were collected as land condition scores (A, B, C or D) for random 1 km buffer circles along the roads from 2004 to 2012, which present three general land conditions from 'Non-decrease' to 'Potential decrease' to 'Significant decrease'. As a result, the following pre-processings were required before the final calculation of the population error matrix: 1) As around 2/3 of the data were collected in the year of 2011 and evenly distributed across the Burdekin region, we re-ran our mapping approach to create a second vegetation cover change map of 2011 in order for it to be validated by these 2011 observations (over 500 points); 2) We aggregated our classified land condition categories into three general classes to match the reference data from the field observations as 'Significant increase', 'Potential increase' and 'Stable' classes correspond to the stable land conditions (A and B), 'Potential decrease' corresponds to the C condition and 'Significant decrease' class is for the D condition; 3) To compare with the field land condition class

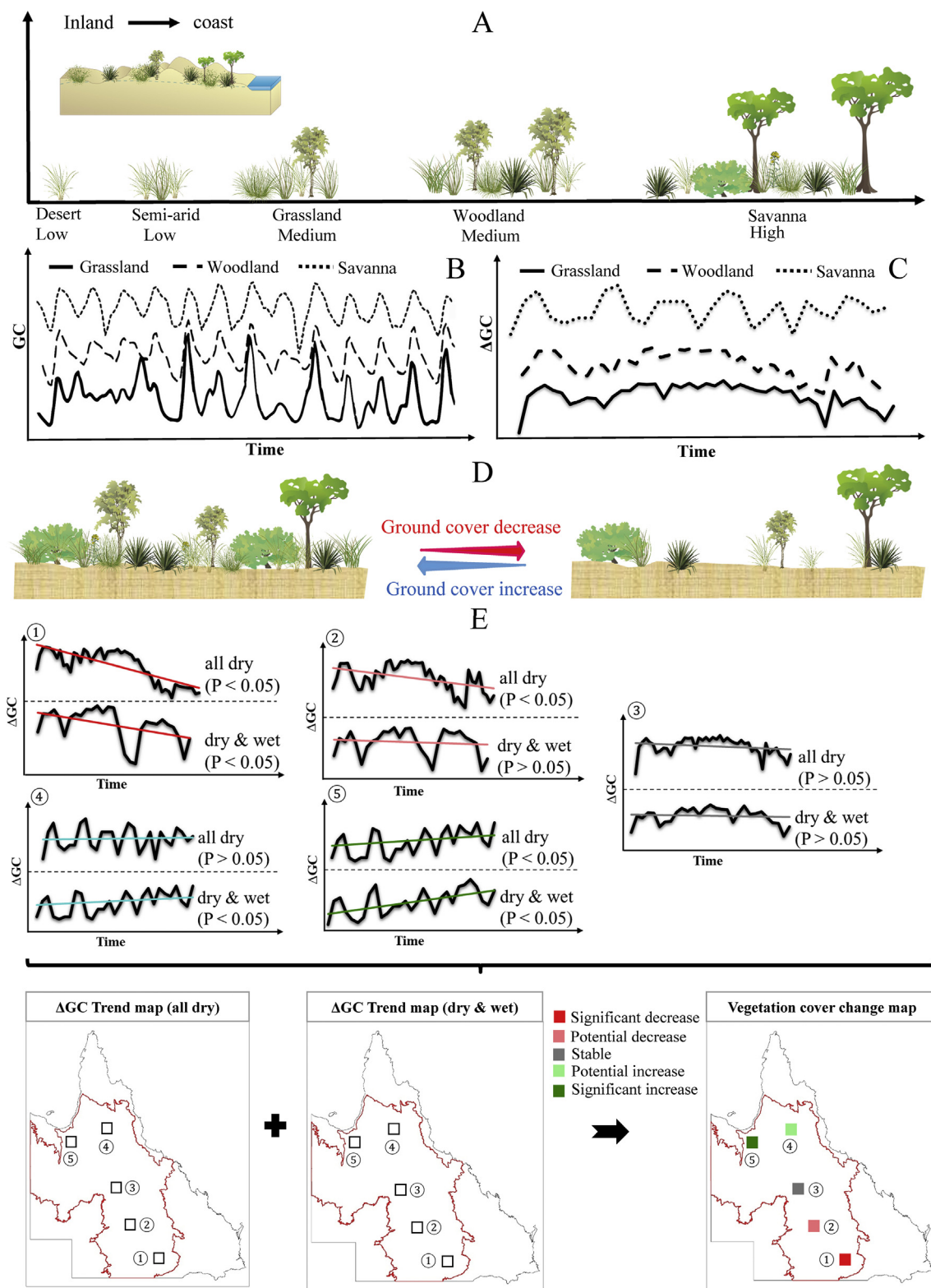


**Fig. 3.** The conceptual diagram of vegetation cover change mapping in this study. (A) Vegetation types in QLD from inland to coast with low to high vegetation ground cover; (B) Ground cover (GC) profiles of major vegetation types (grassland, woodland and savanna); (C) Rainfall adjusted ground cover ( $\Delta GC$ ) profiles of major vegetation types; (D) Illustration of decrease and increase in vegetation ground cover; (E) Final vegetation cover change map determined from two ground cover trend maps based on two time series (successive dry period, both dry and wet years).

for each 1 km buffer circle, we assigned its corresponding classified category by determining the dominant class from our vegetation cover change map that has the most pixels within the circle. Lastly, these aggregated class values can be used as a comparison against the

reference observations across all buffer circles.

All of the experimental datasets in this study (if not already on GEE) were added to the 'Assets' of GEE using Python API of batch uploading (Roy, 2017). The vegetation cover change mapping approach with

**Table 3**

Population error matrix with cell entries ( $P_{ij}$ ) expressed in terms of proportion of area in the mapped class  $i$  and the reference class  $j$ . The equations used to estimate population error matrix, user's accuracy, producer's accuracy, overall accuracy and associated standard errors of the estimators.

Classified	Reference					
		1	2	...	m	Total
1	$P_{11}$	$P_{12}$	...	$P_{1m}$	$P_{1+}$	
2	$P_{21}$	$P_{22}$	...	$P_{2m}$	$P_{2+}$	
.	.	.	...	.	.	
.	.	.	...	.	.	
m	$P_{m1}$	$P_{m2}$	...	$P_{mm}$	$P_{m+}$	
Total	$P_{+1}$	$P_{+2}$	...	$P_{+m}$		

Equation	Comments
$W_i = \frac{A_i}{A_{total}}$	$W_i$ is the proportion of the mapped area of class $i$ in the map. $A_i$ is the mapped area of class $i$ . $A_{total}$ is the total area of the study area.
$P_{ij} = W_i \frac{n_{ij}}{n_{i+}}$	$n_{ij}$ is the number of pixels mapped to class $i$ and belong to category $j$ in the reference data. $P_{ij}$ in cell $i,j$ of the error matrix represents the probability that a randomly selected area is classified to class $i$ and belongs to the class $j$ in the reference data.
$P_{i+} = \sum_{j=1}^m P_{ij} = W_i$	$P_{i+}$ is the estimated proportion of the area of class $i$ in the map that is equal to $W_i$ . $m$ is the number of total classes.
$P_{+j} = \sum_{i=1}^m P_{ij}$	$P_{+j}$ is the proportion of the area of class $j$ as determined from a reference data.
$O = \sum_{j=1}^m P_{jj}$	$O$ (overall accuracy) is the proportion of the area mapped correctly.
$U_i = \frac{P_{ii}}{P_{i+}}$	$U_i$ (user's accuracy) is the proportion of the area mapped as class $i$ that has reference class $i$ .
$W_j = \frac{P_{jj}}{P_{+j}}$	$P_j$ (producer's accuracy) is the proportion of the area of reference class $j$ that is mapped as class $j$ .

The standard error at 95% level of the accuracy measure was calculated as the square root of the estimated variance of the estimators.

ensemble methods was achieved by GEE APIs with access to high-performance, intrinsically parallel computation service (Gorelick et al., 2017).

### 3. Results

#### 3.1. Mapping results for the Wambiana grazing trial area

After the removal of effects from the inter-annual variability in rainfall, the time series of seasonally rainfall adjusted ground cover ( $\Delta GC$ ) during the study period (1988–2017) showed fluctuations that closely followed the long-term hydroclimatic trends indicated by the seasonal SPEI (Fig. 4A). Fig. 4A clearly indicated Australia's recent mega-droughts such as the prolonged Millennium drought (2001 to 2007) and the 2015 El Niño drought. In particular, the resilience of ground cover to environmental stress (i.e. droughts), quantified by the trends and magnitude of loss in  $\Delta GC$  time series, showed ground cover over Wambiana was sensitive to the drought conditions (when SPEI was below the drought threshold line). Ground cover of the paddocks with different grazing strategies was only separable during the dry conditions, presenting distinct responses to the droughts (Fig. 4A). It had the weakest resilience in heavy stocking rate trials (HSR\_1 and HSR\_2), followed by those in the moderate stocking rate trials (MSR\_1 and MSR\_2), while the least decline was evident over the Exclosure area (Exc). These ground cover change time series over the Wambiana grazing trials also revealed wet season or years represented by the positive SPEI (Fig. 4A) offset the effect of management strategies in actual ground cover space. This may result in a failure of using direct trend analysis over the entire time series of  $\Delta GC$  in detecting significant or potential decrease in vegetation cover.

Thus, two sub time series of 1) all successive dry periods (Fig. 4B)

and 2) winter season in all dry and wet years (Fig. 4C) were filtered to solve this issue. HSR and MSR showed significant decline in ground cover during the all dry periods (Fig. 4B) while these downward trends either stayed significant (e.g. HSR\_1 and HSR\_2) or turned to be non-significant (e.g. MSR\_1 and MSR\_2) in the time series of both dry and wet years (Fig. 4C). By contrast, Exc ground cover was able to stay relatively stable in both periods. These results indicated the overall 'Significant decrease' or 'Potential decrease' vegetation cover status under the HSR and MSR grazing trials, both have reduced resilience to drought conditions compared with the Exc area.

Results from  $\Delta GC$ -rainfall correlation analysis showed that the reference vegetation cover of the Wambiana area was significantly correlated with rainfall (Fig. 4D), reflecting the high association between ground cover and rainfall. Moreover, annual  $\Delta GC$  over HSR paddocks was found to be significantly correlated with rainfall while those over the MSR and Exc areas were not. As a result, the significant correlation of the already rainfall adjusted  $\Delta GC$  with rainfall should be largely attributed to human management effect. Thus, this relationship can be potentially used for solving the non-significant trend issue in identifying land degradation, when there was < 20% vegetation deduction during the study time (Wessels et al., 2012). In addition, the accumulative  $\Delta GC$  was shown to effectively identify lands (e.g. Exc area in Wambiana) that showed non-significant trend but had positive accumulation in ground cover through time, which were classified as 'Potential increase' class in this study (green line in Fig. 4E).

A random selection of 1000 Landsat pixels in each vegetation cover change mapping class across the Wambiana area were chosen to assess the  $\Delta GC$  trend during the 'all dry periods' vs during the 'dry and wet years' at the pixel level (Fig. 5A). This scatterplot revealed distinct drought-wet response patterns of ground cover, with pixels under the same vegetation change class clustering together. It also indicated a more reduced resilience of 'Significant decrease' class than 'Potential decrease' class to the changes in the environmental conditions (e.g. wet to dry). Moreover, the close adjacent characteristic between vegetation cover change classes hints at the "rolling ball concept of land condition" (Fig. 25 in Quirk and McIvor, 2003), for example, without effective action being taken, 'Potential decrease' lands are subject to falling into the 'Significant decrease' vegetation cover class (Fig. 5A).

Spatially, these clusters of pixels formed the vegetation cover change map over the Wambiana paddocks with different grazing strategies (Fig. 5B). Areas under a heavy stocking rate i.e. HSR\_1 and HSR\_2 were almost fully covered by 'Significant decrease' and 'Potential decrease' lands. Moderate stocking rate areas (MSR\_1 and MSR\_2) were in a better land condition, showing vegetation cover decrease classes only concentrated in the north the 'box land type' while 'Stable' and 'Potential increase' classes were found over the south part with 'Brigalow and Ironbark land types' (Fig. 1D). The decrease in MSR areas might be partly due to Cattle's strong selective grazing at the patch and certain land type scale (e.g. box land type) irrespective of the level of pasture utilisation reported by the Wambiana grazing report (O'Reagain and Bushell, 2011). By contrast, the Exc area is separated from its surroundings and exhibited as mostly 'Potential increase' land. This map of vegetation cover changes over the Wambiana grazing trial largely corroborated the key results of land conditions described in the Wambiana grazing reports (O'Reagain and Bushell, 2011, 2015).

#### 3.2. Vegetation cover change map of Queensland rangelands

The vegetation cover change mapping approach tested over the Wambiana was applied to the entire study area to produce the final vegetation cover change map of QLD rangelands with five classes: non-decrease vegetation cover of 'Stable', 'Potential increase' and 'Significant increase' classes; decrease vegetation cover of 'Potential decrease' and 'Significant decrease' classes (Fig. 6A). In total, 20% of the study areas were observed to have decrease vegetation cover with 7.5% and 12.4% being in 'Significant decrease' and 'Potential decrease'

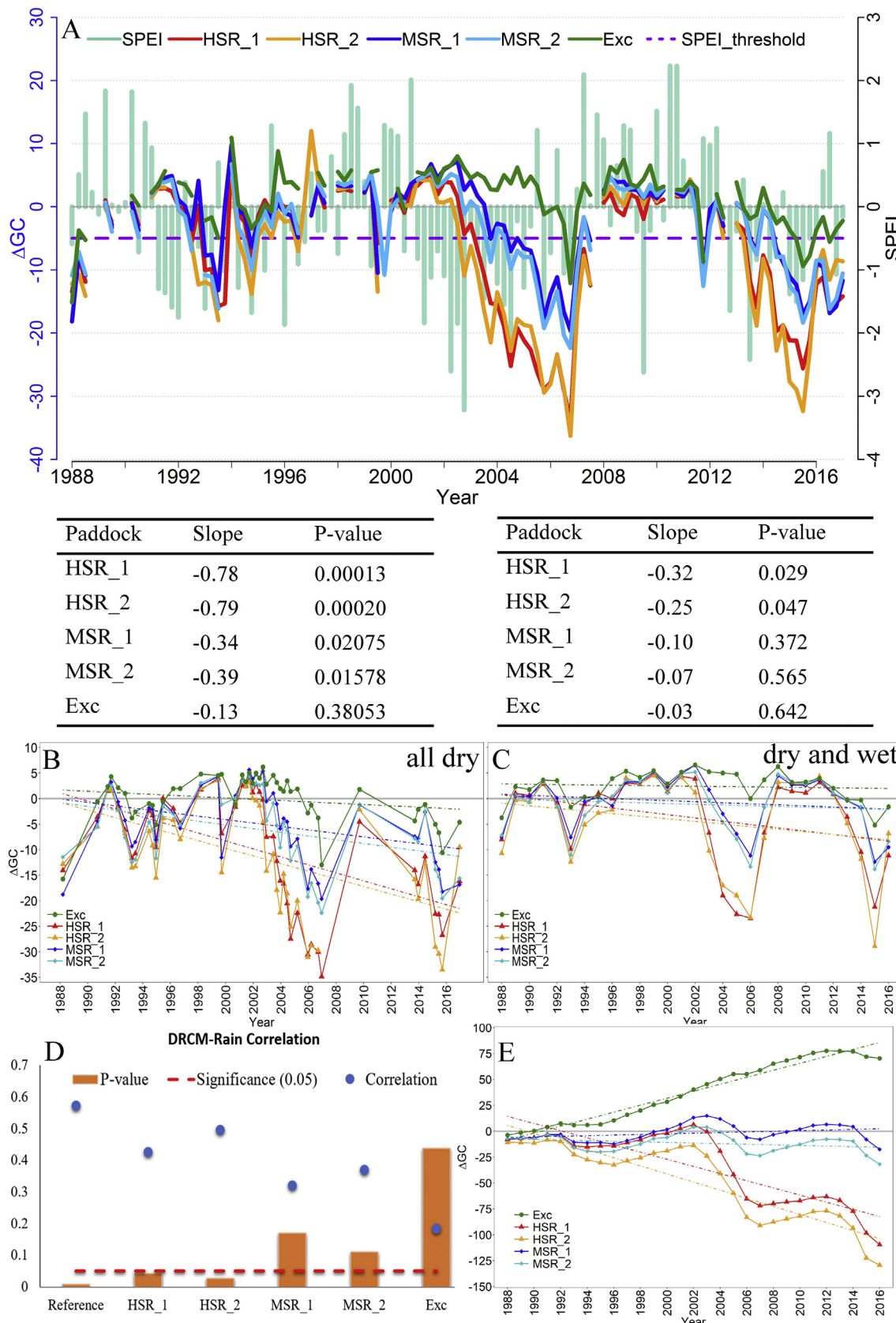


**Fig. 4.** (A) Rainfall adjusted vegetation ground cover ( $\Delta GC$ ) aggregated over five paddocks under three grazing strategies (HSR, MSR and Exc) and seasonal SPEI values over the Wambiana area from 1988 to 2017, with the purple line representing the SPEI drought threshold. (B) Time series of  $\Delta GC$  in all successive dry periods and (C) in winter season during both dry and wet years over the five paddocks with trend lines and regression statistics table (slope and P-value). (D) Correlations (blue points) and P-value (orange histograms) between annual rainfall and  $\Delta GC$  over five paddocks from the start of the grazing trial in 1998 to 2016. (E) Accumulated annual  $\Delta GC$  values aggregated over the five paddocks from 1988 to 2016. (For interpretation of the references to colour in this figure legend, the reader is referred to the web version of this article.)

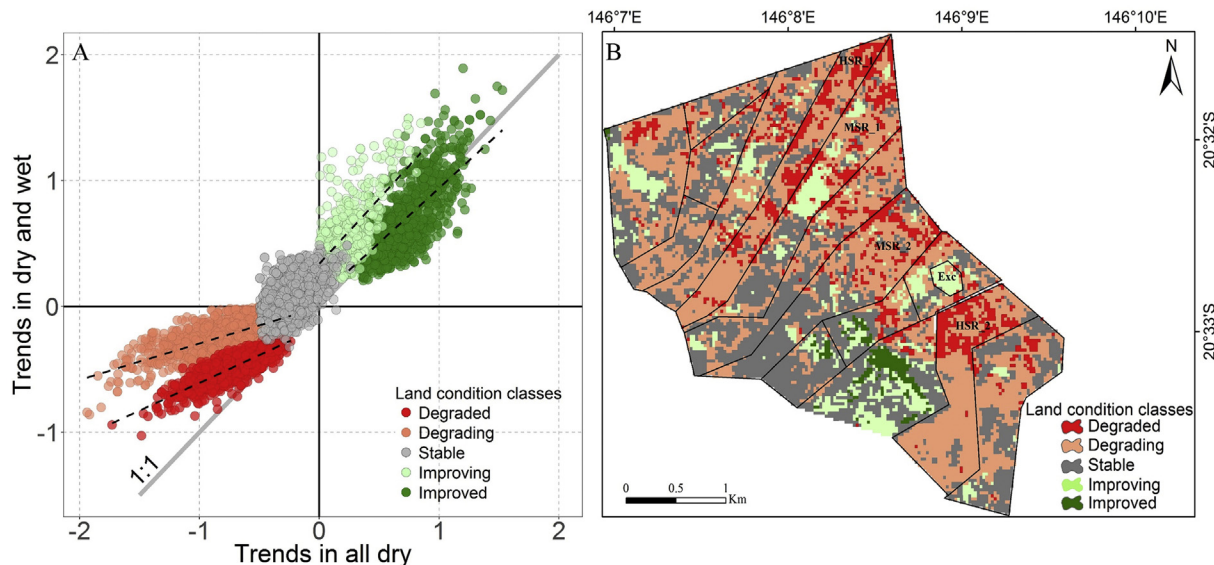


**Fig. 5.** (A) Scatter plot of the  $\Delta GC$  trends during the ‘all dry periods’ (x-axis) vs during the ‘winter in dry and wet years’ (y-axis) derived from random 1000 Landsat pixels in each vegetation cover change class across the Wambiana area. (B) Vegetation cover change map over the Wambiana grazing trial with five classes: ‘Significant decrease’, ‘Potential decrease’, ‘Stable’, ‘Potential increase’ and ‘Significant increase’.

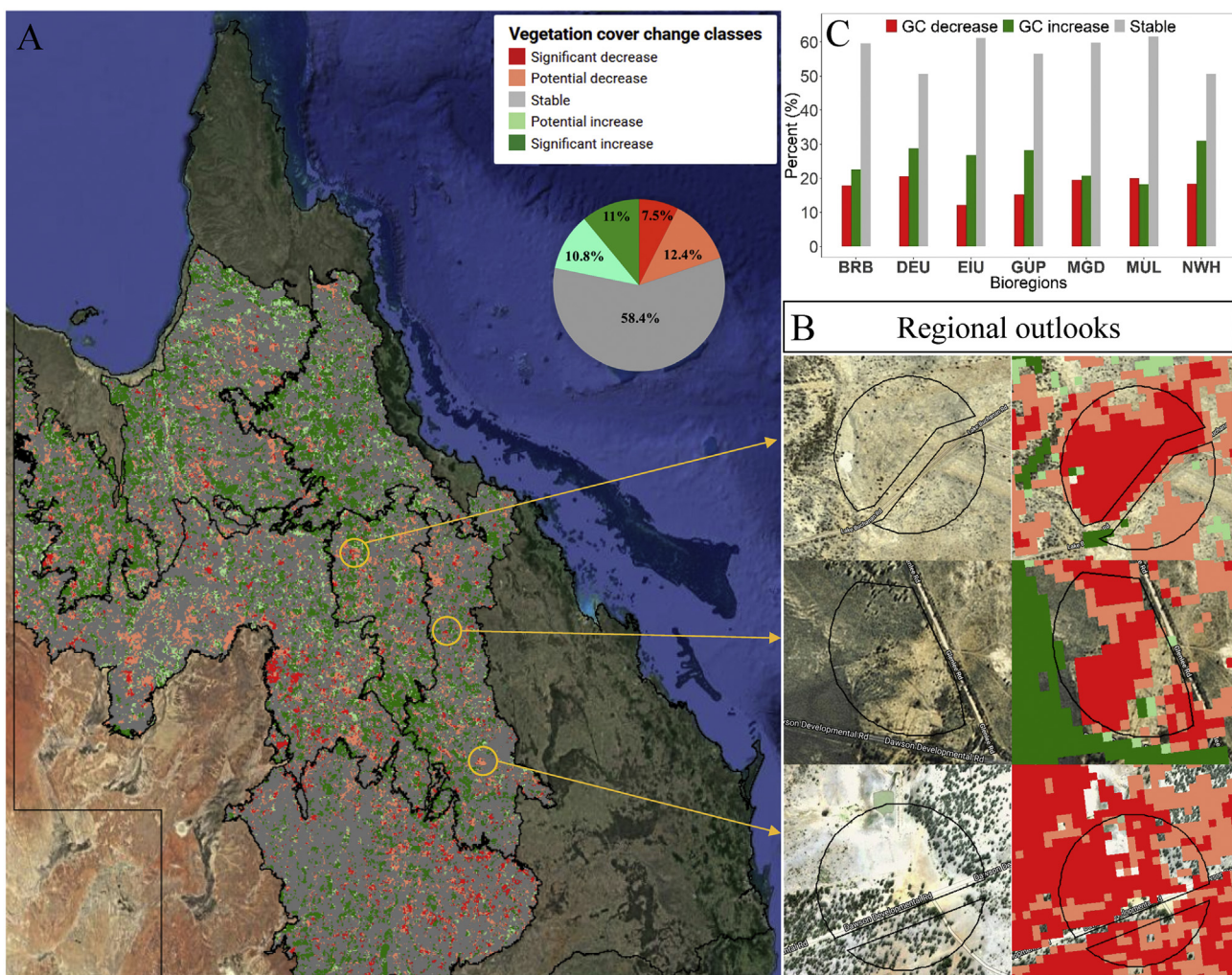


**Fig. 6.** (A) Vegetation cover change map of QLD rangelands with five classes: ‘Significant decrease’, ‘Potential decrease’, ‘Stable’, ‘Potential increase’ and ‘Significant increase’. The black boundary represents the bioregions that cover the entire study area and the pie chart indicates the statistics of the vegetation cover change classes across the study area. (B) Regional outlooks of three ‘Significant decrease’ class sites, which are located in the field 1 km buffer areas with land condition scored as “D:severe land condition decline” (‘Stable’ class was excluded). (C) Statistics of vegetation cover changes across different bioregions.

classes, respectively. Another similar percentage of lands was shown to have increase in vegetation cover by our map (21.8%), with the remaining 58.4% vegetation cover of the study area staying stable (pie chart in Fig. 6A).

Although the major parts of the study area stayed stable during our study period, the areas of decrease vegetation cover took up a considerable area of  $\sim 2.1 \times 10^5 \text{ km}^2$ . These areas, often adjacent to each other, were largely in the form of specks distributed all over our study area, of which the size ranged from 10 to  $650 \text{ km}^2$  (on average  $\sim 3000$  football fields). Several examples of 'Significant decrease' vegetation cover on the map were selected from the validation sites of the 1 km buffer areas with land condition scored as "D:severe land condition decline" (Fig. 6B). The overall mapped classes corresponded well with the field records on the land conditions (Fig. 6B). In general, all the seven bioregions analysed had similar level of vegetation cover changes, with over 50% stable lands and relatively more vegetation cover increase than decrease (Fig. 6C). The Einasleigh Uplands (EIU) and Gulf Plains (GUP) had less decrease in vegetation cover than other assessed bioregions, suggesting they were in a relatively better state based on grazing history. Mitchell Grass Downs (MGD), eastern Mulga Lands (MUL) and north part of the Brigalow Belt (BRB) had the highest percent of vegetation cover decrease ( $\sim 20\%$ ) among all bioregions, which may be attributed to more severe historic grazing impact (Fig. 6C). Apart from grazing, some vegetation cover decrease might also be caused by physical and chemical land disturbances such as previous mining activities but this needs to be further explored in future work.

### 3.3. Accuracy assessment results

Standard accuracy assessment (population error matrix as cross-tabulation of the mapped classes vs the reference classes) was undertaken to assess the accuracy of our vegetation cover change map (Table 4). A total of 523 field observations were used in the validation (Fig. 1B), with 339 records being referred as 'Non-decrease' class that takes up 80% of the classified map while 152 and 32 records being referred as 'Potential decrease' and 'Significant decrease' classes that account for 12.4% and 7.5% of the study area (Table 4). The assessment results yielded an overall classification accuracy of 82.6% ( $\pm 3.32\%$ ). The highest producer's and user's accuracies were found in the 'Non-decrease' class, which were 86.6% ( $\pm 3.59\%$ ) and 94.4% ( $\pm 1.67\%$ ), respectively. The 'Significant decrease' class was observed to be less accurately classified, suggested by the 75% user's accuracy with a relatively lower, 70% producer's accuracy. This confusion should have mostly resulted from the 'Potential decrease' class, which as a transitional vegetation cover change class between 'Non-decrease' and 'Significant decrease' classes, showing the lowest match with the reference data ( $74.8\% \pm 6.92\%$  and  $50.3\% \pm 7.78\%$  for producer's and user's accuracies).

## 4. Discussion

### 4.1. Improving vegetation cover change mapping with 'big data' solutions

Our data and methods provide a first step towards operational mapping vegetation cover changes with a focus on Rangelands, which represent the largest land surface area of any environments. The approach applied in this work using the Google Earth Engine 'big data' techniques and repository enabled efficient data access and processing on otherwise computational intensive tasks, with a total processing time for the study area at pixel level taking less than 5 min. By contrast, conducting the same study without GEE using traditional image processing would require: 1) two Terabytes of memory, 2) a processing time of  $\sim 2$  months (parallel computing of split tiles on HPC), and 3) a storage cost of 150G (compressed GeoTiff format) plus other hidden costs such as time and effort spent on data selecting, acquiring, downloading, mosaicking and image quality control. GEE also makes collaborating and sharing scripts efficient, along with providing easy access to output images and summary analytics through Google Earth Engine App. This will allow data analysts in conservation and land management agencies to apply the code, and for scientists and managers to view and query the results without having to purchase data and software.

Apart from the GEE cloud computing technique, methods used in this study also show improvements on previous studies. For example, we utilized the dynamic reference cover method to objectively separate management effects from those due to inter-annual rainfall variability. In this way, the long-term trends detected in ΔGC in this study can be largely attributed to human induced land cover change rather than seasonal variability due to rainfall. In addition, we computed the new drought index SPEI at 5 km using Australian BoM meteorological data, which is a ten-fold improvement in scale than the existing global SPEI product and can better determine successive dry periods. This multi-scalar drought metric has advantages over other drought indices as it not only incorporates rainfall as an input variable, but also considers temperature and evapotranspiration to accommodate for water losses more accurately.

Previous studies have shown ground cover that persists under environmental stress (e.g. drought) provides protection against erosion and efficiency of biogeochemical cycling, with flow-on benefits to ecosystem productivity and biodiversity (Alcaraz-Segura et al., 2009; Bartley et al., 2010a; Bartley et al., 2010b; Ludwig et al., 2007). In this study, we used total vegetation ground cover as an indicator of environmental condition, based on the well-founded ecological concept that persistent ground cover of native species generally indicates good land condition and high landscape functionality (Bastin et al., 2012). However, this does not provide stakeholders with a complete view on land condition, which also requires other biophysical and socio-economic information. Moreover, being confined by our study period of 1988 to 2017, mapping methods proposed here only apply to the lands that are actively affected by the ongoing processes of vegetation cover decrease since 1988.

A limitation of this study lies in the underlying dynamic reference

**Table 4**

The population error matrix with overall, user's and producer's accuracies of 'Non-decrease', 'Potential decrease' and 'Significant decrease' classes from the vegetation cover change map of QLD rangelands. Standard errors of the estimates are provided in parentheses.

Class (map)	Reference (ground truth)			Accuracy assessment <sup>a</sup> , %			
	Non-decrease	Potential decrease	Significant decrease	$P_{i+} = W_i$	$U_i$	$P_i$	O
Non-decrease	0.6938	0.0839	0.0233	0.801	86.6 ( $\pm 3.59\%$ )	94.4 ( $\pm 1.67\%$ )	82.6 ( $\pm 3.32\%$ )
Potential decrease	0.0304	0.0928	0.0008	0.124	74.8 ( $\pm 6.92\%$ )	50.3 ( $\pm 7.78\%$ )	
Significant decrease	0.0107	0.0080	0.0563	0.075	75.0 ( $\pm 5.16\%$ )	70.0 ( $\pm 4.13\%$ )	
$P_{+j}$	0.7349	0.1847	0.0804				

<sup>a</sup> User's accuracy ( $U_i$ ), producer's accuracy ( $P_i$ ), the overall accuracy (O) and  $W_i$  (proportion of class's area) are described in Table 3.

cover method, which was initially designed for rangeland environment and may not apply well in cropland areas, channel country, and high rainfall zones and so on. Our study focussed on where the initial assumptions of the dynamic reference cover method are valid. Future work with similar styles of reference methods but different data is needed to extend the capability of monitoring land conditions to other environments. For example, ground cover changes in cropping regions could be better assessed by biomass trends over time while those in non-water limited areas could be assessed through the changes in highly bare ground. In addition, even in rangeland areas, uncertainties could still exist in DRCM-derived rainfall adjusted ground cover data. For example, changes in ecosystem's resilience may cause shifts in species composition (Ponce Campos et al., 2013).

#### 4.2. Vegetation cover change mapping as a start for land condition and degradation assessment

The vegetation cover change mapping results were validated using an independent dataset of over 500 field land condition observations across an area of 69,000 km<sup>2</sup>. Results showed that overall accuracy was over 80%, with user's accuracy (complement of commission error) for the 'Significant decrease' and 'Potential decrease' classes being 75% and 74.8% while producer's accuracy (complement of omission error) being 70% and 50.3%. These accuracy measure are commensurate with previous studies on mapping land surface changes over small areas using moderate to high-spatial resolution satellite data (Dimobe et al., 2015; Gao and Li, 2017; Lu et al., 2007; Vågen et al., 2016; Žížala et al., 2017). There are differences between our produced map (30-m vegetation cover changes) and the validation data (1 km buffers with both soil and vegetation condition changes), and while we recognize that uncertainties may exist in our accuracy assessment, these field observations are the best on offer validation data available. Apart from vegetation cover decrease, 80% of the study area were observed either recovering (ca.20%) or being stable (ca.60%) during our study period.

Despite the increasing pressures on already limited land resources, worldwide strategies for solving and understanding land management issues are hindered by missing and often unreliable spatial information on the location, area, and types of vegetation cover changes occurring, and how they are used to define "condition" or "degradation" (Gibbs and Salmon, 2015). This is partly attributed to the challenges of defining "degradation", which likely contributes to the apparent variance in mapping degraded lands (Lamb et al., 2005; Plesník et al., 2011). Moreover, different cultural contexts may add further complexity, making it hard to define and measure land degradation, and to obtain definitive statistics on its regional, national or global scale (Hobbs, 2016). Most previous research in this area has focused on soil degradation, which is difficult to assess due to a lack of suitable soil data. Our vegetation cover change mapping approach will provide a start for land condition and degradation assessment with baseline information at appropriate spatial and temporal scales, which can potentially support conservation policy and management in Australia and other parts of the world.

#### 5. Conclusion

In this study, we mapped vegetation cover changes across most of Queensland's rangelands ( $1.0 \times 10^6$  km<sup>2</sup>) using time series of Landsat data, collected on an approximately monthly basis from 1988 to 2017. We focused on identifying and classifying these vegetation cover changes with a set reference level, and the output map can be used to set user-specified threshold for assessing land conditions. Broadly, reliably, effectively and sustainably monitoring vegetation cover changes to further define land degradation is urgently needed for more effective and efficient resource and conservation land management. This study took an important step towards a better understanding of land surface changes over large-scale areas at fine spatial resolution by utilizing the

'big data' solution of the Google Earth Engine cloud-computing platform. Our next stages of work to improve mapping vegetation cover changes in order to identify degraded lands for conservation will focus on data, methodology and validation: 1) combine satellite data with socio-economic information; 2) overcome the constraints of DRCM for mapping non-rangeland environments; 3) use more extensive validation with field observations and other land surface change maps that are more available across different environments.

#### Acknowledgements

This work was funded by the Australian Research Council - Discovery Project "Global extent of degraded farm lands and their conservation potential" (ARC-DP170101480). EMM was supported by an ARC Future Fellowship and ZX was supported by ARC-DP and the Natural Science Foundation of China (Project No: 41801262). We are grateful for Peter Scarth's help and advice on this work. The first author also appreciates Mr. Geoffrey Pearce and Mr. Eric Pawsey for their suggestions on the grammar of this paper.

#### References

- Aadhar, S., Mishra, V., 2017. High-resolution near real-time drought monitoring in South Asia. *Sci. Data* 4, 170145.
- ABARES [Australian Bureau of Agriculture and Resource Economics and Sciences], 2015. Addendum to the Guidelines for Land Use Mapping in Australia: Principles, Procedures and Definitions, 4th edition. Australian Bureau of Agricultural and Resource Economics and Sciences, Canberra.
- Ahmad, M., Sinclair, C., Werrity, A., 1988. Log-logistic flood frequency analysis. *J. Hydrol.* 98, 205–224.
- Ajmi, M., Hamza, M., Labiad, M., Yermani, M., Khatra, N.B., Al-Thubaiti, A., Moharrem, I., El Arrim, A., 2014. Setting up a spatial data infrastructure (SDI) for the ROSELT/OSS network. *J. Geogr. Inf. Syst.* 6, 150.
- Alcaraz-Segura, D., Cabello, J., Paruelo, J.M., Delibes, M., 2009. Use of descriptors of ecosystem functioning for monitoring a national park network: a remote sensing approach. *Environ. Manag.* 43, 38–48.
- Andeltova, L., Barbier, E., Baker, L., Shim, K., Noel, S., Quatrini, S., Schauer, M., 2013. The rewards of investing in sustainable land management. In: Interim Report for the Economics of Land Degradation Initiative: A Global Strategy for Sustainable Land Management. Bonn, Germany.
- Australian Bureau of Meteorology, 2018. Australian daily rainfall gridded data (recalibrated). <http://www.bom.gov.au/climate/how/newproducts/IDCdrgrids.shtml>, Accessed date: 8 January 2018.
- Ayala-Izurieta, J., Márquez, C., García, V., Recalde-Moreno, C., Rodríguez-Llerena, M., Damián-Carrión, D., 2017. Land cover classification in an Ecuadorian Mountain geosystem using a random Forest classifier, spectral vegetation indices, and ancillary geographic data. *Geosciences* 7, 34.
- Bai, Z.G., Dent, D.L., Olsson, L., Schaepman, M.E., 2008. Proxy global assessment of land degradation. *Soil Use Manag.* 24, 223–234.
- Bartley, R., Corfield, J.P., Abbott, B.N., Hawdon, A.A., Wilkinson, S.N., Nelson, B., 2010a. Impacts of improved grazing land management on sediment yields, part 1: hillslope processes. *J. Hydrol.* 389, 237–248.
- Bartley, R., Wilkinson, S.N., Abbott, B.N., Post, D.A., 2010b. Impacts of improved grazing land management on sediment yields. Part 2: catchment response. *J. Hydrol.* 389, 249–259.
- Bastin, G., Scarth, P., Chewings, V., Sparrow, A., Denham, R., Schmidt, M., O'Reagain, P., Shepherd, R., Abbott, B., 2012. Separating grazing and rainfall effects at regional scale using remote sensing imagery: a dynamic reference-cover method. *Remote Sens. Environ.* 121, 443–457.
- Batjes, N., 2001. Soil data resources for land suitability assessment and environmental protection in central and eastern Europe: the 1: 2,500,000 scale SOVEUR project. *The Land* 5, 51–68.
- Bedunah, D.J., Angerer, J.P., 2012. Rangeland degradation, poverty, and conflict: how can rangeland scientists contribute to effective responses and solutions? *Rangel. Ecol. Manag.* 65, 606–612.
- Beguería, S., Vicente-Serrano, S.M., Reig, F., Latorre, B., 2014. Standardized precipitation evapotranspiration index (SPEI) revisited: parameter fitting, evapotranspiration models, tools, datasets and drought monitoring. *Int. J. Climatol.* 34, 3001–3023.
- Butchart, S.H., Clarke, M., Smith, R.J., Sykes, R.E., Scharlemann, J.P., Harfoot, M., Buchanan, G.M., Angulo, A., Balmford, A., Bertzky, B., 2015. Shortfalls and solutions for meeting national and global conservation area targets. *Conserv. Lett.* 8, 329–337.
- Caccetta, P., Dunne, R., George, R., McFarlane, D., 2010. A methodology to estimate the future extent of dryland salinity in the southwest of Western Australia. *J. Environ. Qual.* 39, 26–34.
- Cai, X., Zhang, X., Wang, D., 2010. Land availability for biofuel production. *Environ. Sci. Technol.* 45, 334–339.
- Congalton, R.G., 1991. A review of assessing the accuracy of classifications of remotely sensed data. *Remote Sens. Environ.* 37, 35–46.
- Dimobe, K., Ouédraogo, A., Soma, S., Goetze, D., Porembski, S., Thiombiano, A., 2015.

- Identification of driving factors of land degradation and deforestation in the Wildlife Reserve of Bontioli (Burkina Faso, West Africa). *Glob. Ecol. Conserv.* 4, 559–571.
- Donchyts, G., Baart, F., Winsemius, H., Gorelick, N., Kwadijk, J., van de Giesen, N., 2016. Earth's surface water change over the past 30 years. *Nat. Clim. Chang.* 6, 810–813.
- Dregne, H.E., 2002. Land degradation in the drylands. *Arid Land Res. Manag.* 16, 99–132.
- Eckert, S., Hüsler, F., Liniger, H., Hodel, E., 2015. Trend analysis of MODIS NDVI time series for detecting land degradation and regeneration in Mongolia. *J. Arid Environ.* 113, 16–28.
- Flood, N., 2013. Seasonal composite Landsat TM/ETM+ images using the medoid (a multi-dimensional median). *Remote Sens.* 5, 6481–6500.
- Foody, G.M., 2002. Status of land cover classification accuracy assessment. *Remote Sens. Environ.* 80, 185–201.
- Furby, S., Caccetta, P., Wallace, J., 2010. Salinity monitoring in Western Australia using remotely sensed and other spatial data. *J. Environ. Qual.* 39, 16–25.
- Gao, J., Li, X., 2017. A knowledge-based approach to mapping degraded meadows on the Qinghai-Tibet plateau, China. *Int. J. Remote Sens.* 38, 6147–6163.
- Gibbs, H., Salmon, J., 2015. Mapping the world's degraded lands. *Appl. Geogr.* 57, 12–21.
- Gill, T., Johansen, K., Phinn, S., Trevithick, R., Scarth, P., Armstrong, J., 2017. A method for mapping Australian woody vegetation cover by linking continental-scale field data and long-term Landsat time series. *Int. J. Remote Sens.* 38, 679–705.
- Goodwin, N.R., Collett, L.J., Denham, R.J., Flood, N., Tindall, D., 2013. Cloud and cloud shadow screening across Queensland, Australia: an automated method for Landsat TM/ETM+ time series. *Remote Sens. Environ.* 134, 50–65.
- Gorelick, N., Hancher, M., Dixon, M., Ilyushchenko, S., Thau, D., Moore, R., 2017. Google Earth Engine: planetary-scale geospatial analysis for everyone. *Remote Sens. Environ.* 202, 18–27.
- Han, D., Wang, G., Liu, T., Xue, B.-L., Kuczera, G., Xu, X., 2018. Hydroclimatic response of evapotranspiration partitioning to prolonged droughts in semiarid grassland. *J. Hydrol.* 563, 766–777.
- Hansen, M.C., Loveland, T.R., 2012. A review of large area monitoring of land cover change using Landsat data. *Remote Sens. Environ.* 122, 66–74.
- Hansen, M.C., Potapov, P.V., Moore, R., Hancher, M., Turubanova, S., Tyukavina, A., Thau, D., Stehman, S., Goetz, S., Loveland, T., 2013. High-resolution global maps of 21st-century forest cover change. *Science* 342, 850–853.
- Hein, L., De Ridder, N., Hiernaux, P., Leemans, R., De Wit, A., Schaeffer, M., 2011. Desertification in the Sahel: towards better accounting for ecosystem dynamics in the interpretation of remote sensing images. *J. Arid Environ.* 75, 1164–1172.
- Helldén, U., Tottrup, C., 2008. Regional desertification: a global synthesis. *Glob. Planet. Chang.* 64, 169–176.
- Hestir, E.L., Khanha, S., Andrew, M.E., Santos, M.J., Viers, J.H., Greenberg, J.A., Rajapakse, S.S., Ustin, S.L., 2008. Identification of invasive vegetation using hyperspectral remote sensing in the California Delta ecosystem. *Remote Sens. Environ.* 112, 4034–4047.
- Hobbs, R.J., 2016. Degraded or just different? Perceptions and value judgements in restoration decisions. *Restor. Ecol.* 24, 153–158.
- Holm, A., 2003. The use of time-integrated NOAA NDVI data and rainfall to assess landscape degradation in the arid shrubland of Western Australia. *Remote Sens. Environ.* 85, 145–158.
- Hubacek, K., Sun, L., 2001. A scenario analysis of China's land use and land cover change: incorporating biophysical information into input-output modeling. *Struct. Chang. Econ. Dyn.* 12, 367–397.
- Huete, A., Didan, K., Miura, T., Rodriguez, E.P., Gao, X., Ferreira, L.G., 2002. Overview of the radiometric and biophysical performance of the MODIS vegetation indices. *Remote Sens. Environ.* 83, 195–213.
- IPBES: Intergovernmental Science-Policy Platform on Biodiversity and Ecosystem Services. 2018. Global Assessment Report on Land Degradation and Restoration. Medellín, Colombia.
- Johansen, K., Phinn, S., Taylor, M., 2015. Mapping woody vegetation clearing in Queensland, Australia from Landsat imagery using the Google Earth Engine. *Remote Sens. Appl. Soc. Environ.* 1, 36–49.
- Jones, D.A., Wang, W., Fawcett, R., 2009. High-quality spatial climate data-sets for Australia. *Aust. Meteorol. Oceanogr. J.* 58, 233.
- Karfs, R., Abbott, B., Scarth, P., Wallace, J., 2009a. Land condition monitoring information for reef catchments: a new era. *Rangel. J.* 31, 69–86.
- Karfs, R., Holloway, C., Pritchard, K., Resing, J., 2009b. Land Condition Photo Standards for the Burdekin Dry Tropics Rangelands: A Guide for Practitioners. Burdekin Solutions Ltd and Queensland Department of Primary Industries and Fisheries, Townsville, Australia.
- Kennedy, R.E., Andréfouët, S., Cohen, W.B., Gómez, C., Griffiths, P., Hais, M., Healey, S.P., Helmer, E.H., Hostert, P., Lyons, M.B., 2014. Bringing an ecological view of change to Landsat-based remote sensing. *Front. Ecol. Environ.* 12, 339–346.
- Lamb, D., Erskine, P.D., Parrotta, J.A., 2005. Restoration of degraded tropical forest landscapes. *Science* 310, 1628–1632.
- Liu, C., Frazier, P., Kumar, L., 2007. Comparative assessment of the measures of thematic classification accuracy. *Remote Sens. Environ.* 107, 606–616.
- Lobell, D.B., 2010. Remote sensing of soil degradation: introduction. *J. Environ. Qual.* 39, 1–4.
- Lu, D., Batistella, M., Mausel, P., Moran, E., 2007. Mapping and monitoring land degradation risks in the Western Brazilian Amazon using multitemporal Landsat TM/ETM+ images. *Land Degrad. Dev.* 18, 41–54.
- Ludwig, J., Tongway, D., 2002. Clearing savannas for use as rangelands in Queensland: altered landscapes and water-erosion processes. *Rangel. J.* 24, 83–95.
- Ludwig, J.A., Bastin, G.N., Chewings, V.H., Eager, R.W., Liedloff, A.C., 2007. Leakiness: a new index for monitoring the health of arid and semiarid landscapes using remotely sensed vegetation cover and elevation data. *Ecol. Indic.* 7, 442–454.
- Lyburner, L., Tan, P., Mueller, N., Thackway, R., Thankappan, M., Islam, A., Lewis, A., Randall, L., Senarath, U., 2011. Land cover map of Australia. In: Scale 1:5 000 000, 1st ed. GeoScience Australia, Canberra.
- Mariano, D.A., Santos, C.A.C., Wardlow, B.D., Anderson, M.C., Schiltmeyer, A.V., Tadesse, T., Svoboda, M.D., 2018. Use of remote sensing indicators to assess effects of drought and human-induced land degradation on ecosystem health in Northeastern Brazil. *Remote Sens. Environ.* 213, 129–143.
- McDonald-Madden, E., Runge, M.C., Possingham, H.P., Martin, T.G., 2011. Optimal timing for managed relocation of species faced with climate change. *Nat. Clim. Chang.* 1, 261.
- Muir, J., Schmidt, M., Tindall, D., Trevithick, R., Scarth, P., Stewart, J., 2011. Guidelines for Field Measurement of Fractional Ground Cover: A Technical Handbook Supporting the Australian Collaborative Land Use and Management Program. Queensland Department of Environment and Resource Management for the Australian Bureau of Agricultural and Resource Economics and Sciences, Canberra.
- Oldeman, L., Hakkeling, R., Sombroek, W.G., 1990. World Map of the Status of Human-Induced Soil Degradation: An Explanatory Note. International Soil Reference and Information Centre/United Nations Environment Programme, Wageningen, The Netherlands.
- Olofsson, P., Foody, G.M., Herold, M., Stehman, S.V., Woodcock, C.E., Wulder, M.A., 2014. Good practices for estimating area and assessing accuracy of land change. *Remote Sens. Environ.* 148, 42–57.
- O'Reagain, P., Bushell, J., 2011. The Wambiana Grazing Trial: Key Learnings for Sustainable and Profitable Management in a Variable Environment. Queensland Government, Brisbane, Australia.
- O'Reagain, P., Bushell, J., 2015. Managing for a Variable Climate: Long-Term Results and Management Recommendations from the Wambiana Grazing Trial. Queensland Government, Brisbane, Australia.
- O'Reagain, P., Bushell, J., Holloway, C., Reid, A., 2009. Managing for rainfall variability: effect of grazing strategy on cattle production in a dry tropical savanna. *Anim. Prod. Sci.* 49, 85–99.
- Pekel, J.-F., Cottam, A., Gorelick, N., Belward, A.S., 2016. High-resolution mapping of global surface water and its long-term changes. *Nature* 540, 418–422.
- Plesník, J., Hosek, M., Condé, S., 2011. A Concept of a Degraded Ecosystem in Theory and Practice—A Review. ETC/BD Working Paper No. A/2011. The European Topic Centre on Biological Diversity (ETC/BD), Paris, France.
- Ponce Campos, G.E., Moran, M.S., Huete, A., Zhang, Y., Bresloff, C., Huxman, T.E., Eamus, D., Bosch, D.D., Buda, A.R., Gunter, S.A., 2013. Ecosystem resilience despite large-scale altered hydroclimatic conditions. *Nature* 494, 349–352.
- Poore, J.A., 2016. Call for conservation: abandoned pasture. *Science* 351, 132.
- Possingham, H.P., Bode, M., Klein, C.J., 2015. Optimal conservation outcomes require both restoration and protection. *PLoS Biol.* 13, e1002052.
- Priestley, C., Taylor, R., 1972. On the assessment of surface heat flux and evaporation using large-scale parameters. *Mon. Weather Rev.* 100, 81–92.
- Quirk, M., McIvor, J., 2003. Grazing Land Management: Technical Manual. Meat and Livestock Australia, Sydney.
- Raupach, M.R., Briggs, P.R., Haverd, V., King, E.A., Paget, M., Trudinger, C.M., 2009. Australian Water Availability Project (AWAP): CSIRO Marine and Atmospheric Research Component: Final Report for Phase 3. CAWCR Technical Report No. 13. (Canberra:Australia).
- Raupach, M.R., Briggs, P.R., Haverd, V., King, E.A., Paget, M., Trudinger, C.M., 2018. Australian water availability project, data release 26m. CSIRO oceans and atmosphere. <http://www.csiro.au/awap/>, Accessed date: 13 February 2018.
- Roy, S., 2017. Google Earth Engine Asset Manager with Addons. (USA).
- Scarth, P., Byrne, M., Danaher, T., Henry, B., Hassett, R., Carter, J., Timmers, P., 2006. State of the paddock: Monitoring condition and trend in groundcover across Queensland. In: Proceedings from the Australasian Remote Sensing and Photogrammetry Conference, 20–24 Nov. Darwin, Australia.
- Scarth, P., Röder, A., Schmidt, M., Denham, R., 2010. Tracking grazing pressure and climate interaction—the role of Landsat fractional cover in time series analysis. In: Proceedings of the 15th Australasian Remote Sensing and Photogrammetry Conference, Alice Springs, Australia, pp. 13–17.
- Scarth, P., Armstrong, J., Flood, N., Denham, R., Collett, L., Watson, F., Trevithick, B., Muir, J., Goodwin, N., Tindall, D., 2015. Operational application of the landsat timeseries to address large area landcover understanding. *Int. Arch. Photogramm. Remote. Sens. Spat. Inf. Sci.* 40, 571.
- Singh, V., Guo, H., Yu, F., 1993. Parameter estimation for 3-parameter log-logistic distribution (LLD3) by pome. *Stoch. Hydraul. Hydraul.* 7, 163–177.
- Sommer, S., Zucca, C., Grainger, A., Cherlet, M., Zougmoré, R., Sokona, Y., Hill, J., Della Peruta, R., Roehrig, J., Wang, G., 2011. Application of indicator systems for monitoring and assessment of desertification from national to global scales. *Land Degrad. Dev.* 22, 184–197.
- Swinbank, W.C., 1963. Long-wave radiation from clear skies. *Q. J. R. Meteorol. Soc.* 89, 339–348.
- Tewkesbury, A.P., Comber, A.J., Tate, N.J., Lamb, A., Fisher, P.F., 2015. A critical synthesis of remotely sensed optical image change detection techniques. *Remote Sens. Environ.* 160, 1–14.
- Trevithick, R., Muir, J., Denham, R., 2012. The effect of observer experience levels on the variability of fractional ground cover reference data. In: Proceeding of the 16th Annual ARSPC, Melbourne, Australia.
- Trevithick, R., Scarth, P., Tindall, D., Denham, R., Flood, N., 2014. Cover under Trees: Rp64g Synthesis Report. Department of Science, Information Technology, Innovation and the Arts, Brisbane, Queensland, Australia.
- Turner, K.G., Anderson, S., Gonzales-Chang, M., Costanza, R., Courville, S., Dalgaard, T., Dominati, E., Kubiszewski, I., Ogilvy, S., Porfirio, L., Ratna, N., Sandhu, H., Sutton, P.C., Svensson, J.-C., Turner, G.M., Varennes, Y.-D., Voinov, A., Wratten, S., 2016. A review of methods, data, and models to assess changes in the value of ecosystem

- services from land degradation and restoration. *Ecol. Model.* 319, 190–207.
- Vågen, T.G., Winowiecki, L.A., Tondoh, J.E., Desta, L.T., Gumbrecht, T., 2016. Mapping of soil properties and land degradation risk in Africa using MODIS reflectance. *Geoderma* 263, 216–225.
- Venter, O., Fuller, R.A., Segan, D.B., Carwardine, J., Brooks, T., Butchart, S.H., Di Marco, M., Iwamura, T., Joseph, L., O'Grady, D., 2014. Targeting global protected area expansion for imperilled biodiversity. *PLoS Biol.* 12, e1001891.
- Vicente-Serrano, S.M., Beguería, S., López-Moreno, J.I., 2010. A multiscalar drought index sensitive to global warming: the standardized precipitation evapotranspiration index. *J. Clim.* 23, 1696–1718.
- Vicente-Serrano, S.M., Cabello, D., Tomás-Burguera, M., Martín-Hernández, N., Beguería, S., Azorin-Molina, C., Kenawy, A.E., 2015a. Drought variability and land degradation in semiarid regions: assessment using remote sensing data and drought indices (1982–2011). *Remote Sens.* 7, 4391–4423.
- Vicente-Serrano, S.M., Van der Schrier, G., Beguería, S., Azorin-Molina, C., Lopez-Moreno, J.-I., 2015b. Contribution of precipitation and reference evapotranspiration to drought indices under different climates. *J. Hydrol.* 526, 42–54.
- Vogt, J., Safriel, U., Von Maltitz, G., Sokona, Y., Zougmore, R., Bastin, G., Hill, J., 2011. Monitoring and assessment of land degradation and desertification: towards new conceptual and integrated approaches. *Land Degrad. Dev.* 22, 150–165.
- Watson, I., Novelty, P., Thomas, P., 2007. Monitoring changes in pastoral rangelands—the Western Australian Rangeland Monitoring System (WARMS). *Rangel. J.* 29, 191–205.
- Watson, J.E., Dudley, N., Segan, D.B., Hockings, M., 2014. The performance and potential of protected areas. *Nature* 515, 67–73.
- Wessels, K.J., Prince, S.D., Carroll, M., Malherbe, J., 2007. Relevance of rangeland degradation in semiarid northeastern South Africa to the nonequilibrium theory. *Ecol. Appl.* 17, 815–827.
- Wessels, K.J., Van Den Bergh, F., Scholes, R., 2012. Limits to detectability of land degradation by trend analysis of vegetation index data. *Remote Sens. Environ.* 125, 10–22.
- Zhang, J., Foody, G., 1998. A fuzzy classification of sub-urban land cover from remotely sensed imagery. *Int. J. Remote Sens.* 19, 2721–2738.
- Zhu, Z., Woodcock, C.E., 2012. Object-based cloud and cloud shadow detection in Landsat imagery. *Remote Sens. Environ.* 118, 83–94.
- Žížala, D., Zádorová, T., Kapička, J., 2017. Assessment of soil degradation by erosion based on analysis of soil properties using aerial hyperspectral images and ancillary data, Czech Republic. *Remote Sens.* 9, 28.